A Hybrid Intelligent Reflecting Surface with Graphene-based Control Elements for THz Communications

Arjun Singh*, Michael Andrello†‡, Erik Einarsson†§
Ngwe Thawdar‡, Josep M. Jornet*

*Department of Electrical and Computer Engineering
Northeastern University, Boston, MA, USA E-mail: {singh.arj,jmjornet}@northeastern.edu

†Department of Electrical Engineering
§Department of Materials Design and Innovation
University at Buffalo, Buffalo, NY, USA, E-mail: {maandrel,erikeina}@buffalo.edu

‡US Air Force Research Laboratory
Rome, NY, USA, E-mail: ngwe.thawdar@us.af.mil

***Abstract*—Terahertz (THz)-band (0.1-10 THz) communication is envisioned as a key wireless technology to fulfill the demand for increasing data rates and to accommodate denser networks. The THz-band, however, suffers from very high propagation losses further aggravated by the presence of obstacles in common scenarios, that behave as opaque barriers at THz frequencies. Engineering non-line-of-sight (NLoS) communication links with-smart reflectarrays is one possible method of overcoming the complex THz communication model. However, existing reflectarray designs at lower frequencies cannot be simply repurposed due to the operating failure of the traditional control elements at THz frequencies. In this direction, the use of 2D nanomaterials, such as graphene, to design tuning elements and integrate these into THz reflectarrays is being explored. This paper presents a novel graphene-based tuning element for continuous phase control of the reflecting element, in situ. The fundamental radiating element is designed to have high reflection efficiency and tunability by leveraging the properties of metals and graphene, respectively. First, the working principle and design of the proposed tuning element, comprised of a graphene-based plasmonic waveguide, is described and explained. Second, the trade-offs in the design of the hybrid tunable reflecting element, resulting from the integration of the tuning element with a metallic patch, are exhaustively studied. After discussing the integration of multiple reflecting elements in a reflectarray, the ability to perform complete continuous dynamic beamforming is presented.**

***Index Terms*—Terahertz communications; Reflectarrays; Graphene plasmonics; Smart Reflecting Surfaces; Beamforming**

I. Introduction

The continuous expansion of wireless communications, with an ever increasing number of connected devices as well as faster communication rates, requires a bandwidth much higher than that available in the overcrowded portion of the electromagnetic (EM) spectrum utilized in current technological standards. In this light, Terahertz (THz)-band technology has gained the attention of the research community [1], [2]. The THz band, between 0.1–10 THz, has multiple transmission windows up to hundreds of gigahertz (GHz) wide. The proper utilization of such a large spectral resource therefore solves the challenges in supporting the next generation of wireless communications. However, there are several barriers in the exploitation of the THz band, due to which this part of the EM spectrum has remained underutilized. Inter alia, true THz signal sources have low power output (usually in the order of 10–100s μW) that is further crippled by the very high propagation losses at THz frequencies, severely restricting the communication distance [3]. To overcome this *grand challenge* of the THz band, beamforming antenna arrays have been proposed [4]. As successfully demonstrated at lower frequencies [5], these improve radiation efficiency by concentrating the available power into a pencil thin beam directed either along a Line of Sight (LoS) or specular Non-Line of Sight (NLoS) paths between the transmitter and the receiver. Additionally, reconfigurable arrays can enable spatial multiplexing of users, thereby providing support for multiple-input-multiple-output (MIMO) systems.

While success has been demonstrated for THz antenna arrays that increase the radiation efficiency [6], dynamic beamforming arrays at THz frequencies are still under development, due to a lack of tuning and control elements [7]. In this light, the utilization of plasmonic materials, such as graphene, has attracted the attention of the research community. Graphene, a two-dimensional carbon material, is very well suited for propagating extremely high frequency signals [8]. In addition, highly tunable Surface Plasmon Polariton (SPP) waves can propagate on graphene at THz frequencies [4]. These are highly confined EM waves generated at the interface of a dielectric and a conductor, with wavelengths as much as orders of magnitude smaller than their free-space EM counterparts. Building upon these promising properties, novel array architecture mechanisms have been proposed, potentially enabling ultra-massive MIMO (UM-MIMO) [4], [9] with up to 1024×1024 elements on a single chip. The enhancement of the

978-1-7281-5478-7/20/$31.00 ©2020 IEEE

communication ends points for a THz-band communication setup has thus been addressed in a non-trivial manner.

However, such advanced techniques at the communication ends are not sufficient, or even feasible, in all scenarios, as common obstacles act as opaque barriers at THz frequencies. This can result in large signal losses, or worse, even complete signal cut-off. Further, it is impractical to assume sophisticated beamforming architectures for low-cost, low-complexity devices. It is therefore necessary to consider the engineering of several transmission paths for such a communication domain. The implementation of smart reflecting surfaces, in particular reflectarrays, is one such method to help facilitate UM-MIMO systems at THz frequencies [10].

A reflectarray is a reflecting surface composed of radiating elements, with the fundamental physics similar to those of antenna arrays. By controlling the response, or phase, of each radiating element, the reflectarray response is dynamically defined to intercept signals from specific directions and reflect these to a target direction [11], [12]. This relaxes the burden on the communication ends significantly. The fundamental working principle of reflectarrays has been demonstrated at near THz frequencies [13]. However, such designs fall short of a dynamic beamforming response as the tuning elements utilized at lower frequencies, such as variable capacitors that act as electrical "buffers" [14], delay stubs with nano and micro electro-mechanical systems (NEMS/MEMS) [15], and liquid crystals with electrically tunable properties [16], reach operational limits at sub-THz frequencies.

Taking advantage of the properties of graphene, several dynamic reflectarrays are also proposed in the THz-band, as in [17]–[19]. However, these suffer from several drawbacks. On the one hand, a discretized phase response and negligence of the effect of non-normal beam incidence leads to incomplete beamforming support. On the other hand, the mismatch between the momentum of SPP waves on graphene and the free-space EM waves, leads to a weak reflection strength of graphene elements, with unacceptable losses. Both ultimately result in poorly performing reflecting strategies. In this paper, we propose the design of a hybrid metal–graphene reflectarray. We jointly design and integrate a gold patch with a graphene-based stub to form the fundamental element of the reflectarray. This design addresses the aforementioned drawbacks, namely, the lack of phase delay available and the radiation inefficiency. This is done by leveraging the advantageous properties of graphene and metals, i.e., good tunability and good reflection strength, respectively. The remainder of this paper is organized as follows. We present the design of the single element and the resulting reflectarray with multiple such elements integrated in Sec. II. We explain the process of phase control and codebook implementation for dynamic beamforming in Sec. III. We rigorously analyze the performance of the reflectarray to fulfill the demands of UM-MIMO links with full wave finite difference frequency domain (FDFD) numerical simulations, and present our results in Sec. IV. Finally, we conclude our paper in Sec. V.

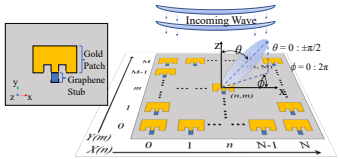

Fig. 1: The hybrid reflectarray with inset showing the single element.

II. Hybrid Reflectarray Design

In this section, we outline the design principles of the hybrid element and its assembly in large arrays. Our design frequency is 1.5 THz (*true* THz frequency), with a free-space wavelength λ_0 of $199.8\,\mu\text{m}$, as this is the center frequency of our experimental setup for future system characterization. Nonetheless, the outlined process is applicable to design the system across the THz band.

A. Single Element Design and Principle

1) Patch: Our design of the metallic patch is derived through the cavity model equations (1) and (2), as per [11]:

$$W = \frac{c}{2f_0\sqrt{\frac{\varepsilon_r+1}{2}}}, \tag{1}$$

$$L = \frac{c}{2f_0\sqrt{\varepsilon_{\text{eff}}}} - 0.824h\left[\frac{(\varepsilon_{\text{eff}}+0.3)(\frac{W}{h}+0.264)}{(\varepsilon_{\text{eff}}-0.258)(\frac{W}{h}+0.8)}\right]. \tag{2}$$

W and L are the width and the length of the patch at a design frequency f_0, and h is the thickness of the substrate. For optimal efficiency at the desired frequency, h is required to be in the range of $0.003 - 0.05\ \lambda_0$, as per [11]. ε_r represents the dielectric constant of the substrate. Since the electric fields of the patch antenna undergo fringing at the boundary of the patch edges, the effective dielectric constant is ε_{eff}, which is found from [11] as:

$$\varepsilon_{\text{eff}} = \frac{\varepsilon_r+1}{2} + \frac{\varepsilon_r-1}{2}[1+12h/W]^{-1/2}. \tag{3}$$

The patch acts as a good reflectarray element through the reciprocity principle: The patch is designed in transmission mode, with resonance at the desired frequency verified through the S11 parameter, or the reflection coefficient [11]. A good transmitter is also a good receiver, and since the reflectarray element works by first receiving and then re-transmitting the signal, the patch is a resonant reflectarray element [12].

2) Stub: We utilize a graphene based stub, that acts as a waveguide with an active graphene layer [20], to implement phase control. The complex SPP wave vector k_{spp} governs the properties of the SPP waves generated in this waveguide. More specifically, the real part $\Re\{k_{\text{spp}}\}$ governs the plasmonic wavelength λ_{spp}, whereas the imaginary part $\Im\{k_{\text{spp}}\}$ sets the decay length D_L:

$$\lambda_{\text{spp}} = \frac{2\pi}{\Re\{k_{\text{spp}}\}}, \tag{4}$$

$$D_L = \frac{1}{2\Im\{k_{\text{spp}}\}}. \tag{5}$$

We utilize the dispersion equation for SPP waves on graphene to derive the wave vector $k_{\rm spp}$ [21]:

$$-i\frac{\sigma^g}{\omega\varepsilon_0} = \frac{\varepsilon_1 + \varepsilon_2 \coth(k_{spp}d)}{k_{spp}}. \tag{6}$$

Here, σ^g is the conductivity of graphene, ε_1 and ε_2 represent the relative permittivities of the dielectrics above (air) and below (silicon dioxide) graphene respectively, while d is the separation between graphene and the ground plane. The conductivity model for graphene can be obtained using the Kubo formalism [22]:

$$\sigma^g = \sigma^g_{intra} + \sigma^g_{inter}. \tag{7}$$

At THz frequencies, the major contribution is through σ^g_{intra}, given as:

$$\sigma^g_{intra} = i\frac{2e^2}{\pi\hbar^2}\frac{k_BT}{\omega + i\tau_g^{-1}}\ln\left[2\cosh\left(\frac{E_F}{2k_BT}\right)\right], \tag{8}$$

which can be further simplified to be:

$$\sigma^g_{intra} = \frac{\tau_g}{1 - i\omega\tau_g}\left(\frac{e^2}{\pi\hbar^2}E_F\right). \tag{9}$$

Here, ω ($2\pi f_0$) is the angular frequency, $\hbar$ is the reduced Planck's constant, e is the electron charge, E_F is the Fermi energy of the graphene sheet (i.e., the highest energy level occupied by electrons in graphene), and τ_g is the relaxation time of electrons in graphene, set as per reported findings [23].

In this setup, we utilize electrostatic bias to change the Fermi energy of the graphene layer, thereby modifying the SPP wave propagation speed. The change in propagation speed leads to a change in the phase of the SPP wave at the output of the stub. The total possible phase difference depends on both the actual physical length L of the stub, as well as the range of Fermi energy considered. This is seen in (10) below, where, for a physical length L of the stub, we derive the relative phase difference Φ_{12} between two SPP waves with different plasmonic wavelengths, the reference at $\lambda_{\rm spp_1}$ for a Fermi energy E_{F_1}, and the other at $\lambda_{\rm spp_2}$ for a Fermi energy E_{F_2}, to be:

$$\Phi_{12} = 2\pi\frac{L}{\lambda_{\rm spp_1}}\left(1 - \frac{\lambda_{\rm spp_1}}{\lambda_{\rm spp_2}}\right). \tag{10}$$

3) Joint Design: We obtain the hybrid building block of the reflectarray by combining the metallic patch and the graphene-based stub. The patch converts an incident wave at the design frequency to an electrical current, generating an SPP wave which propagates across the stub. The SPP wave travels across the length of the graphene stub and back towards the patch, and is re-radiated as an EM wave by the patch.

As first shown in [24], the characteristic impedance of graphene nano-ribbons changes with the Fermi energy, which might lead to an impedance mismatch at the metal–graphene interface. The analytical characterization of this interface is beyond the scope of this work. We instead perform a numerical analysis to determine the optimal design, presented in the inset of Fig. 1 as per the principles outlined. A summary of the dimensions is provided in Table I.

TABLE I: Hybrid Element Dimensions

Substrate permittivity	$4\varepsilon_0$
Substrate thickness	2.3 µm
Patch width	63.2 µm
Patch length	49.94 µm
Stub length	15 µm
Stub width	10 µm
Inlet width	9 µm
Inlet length	18 µm
Graphene relaxation time	1 ps

B. Reflectarray Design and Principle

Our reflectarray design follows traditional array theory – In particular, to negate mutual coupling effects while avoiding grating lobes, we keep the centre to centre spacing between the elements at $\lambda_0/2$ [11]. The hybrid reflectarray is presented in Fig. 1. As is shown, the reflectarray is excited by an incident beam, with a free-space wave number k_0. Through the application of a codebook, we assign every element of the array a certain beamforming weight. The resultant beam from the superposition of all the weighted elements is steered to the desired direction (θ, ϕ). For this operation, the progressive phase delay between the array elements should be Φ_{RA}, where

$$\Phi_{RA} = k_0(R_i - d\sin\theta(\Delta x\cos\phi + \Delta y\sin\phi)). \tag{11}$$

Here, d is the separation between the elements for the array, while setting Δx or Δy to 1 signifies a progression in the x or y direction, respectively. The correction term k_0R_i accounts for the incremental inherent phase delay from the incidence angle of the beam.

III. Reflectarray Control

A. Codebook Design

We implement the required phase delay for each element at position n, m of the array in Fig. 1, as per Eq. (11), by defining a codebook that is composed of effective weights $W_{n,m}$. These correspond to the n, m element and are of the form Ae^{iB}, where A represents the magnitude of signal strength, and B represents the relative phase. For the reflectarray to provide complete continuous beamforming, the weights required are of the form

$$W_{codebook} \in [1e^{i0}, 1e^{i2\pi}]. \tag{12}$$

As described in Sec. II, the codebook can be applied by mapping the effective complex weight $W_{n,m}$ to a particular Fermi energy $EF_{stub_{n,m}}$ of the graphene stub of the (n, m) element:

$$W_{n,m} \mapsto EF_{stub_{n,m}}. \tag{13}$$

B. Codebook Application

To implement the codebook, we first derive the relation between the Fermi energy of the stub and the relative phase delay. Since these have a non-linear relation as shown in (6), we find the variation of the electric field amplitude at the output of the stub as a function of the Fermi energy of the stub, through full wave analysis of a single hybrid element, under

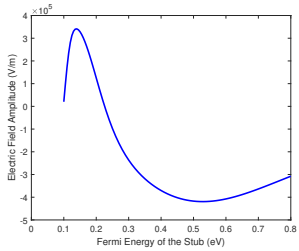

Fig. 2: Electric field amplitude at the output of the graphene-based stub with varying Fermi energy.

transmission mode. Figure 2 presents this relation, where it is seen that for different Fermi energy levels, the corresponding output fields exhibit a phase difference exceeding π radians. In reflection, the phase difference is doubled, and therefore complete phase control with 2π radians is possible.

IV. Results

In this section, we numerically characterize the performance of the hybrid element and reflectarray, in terms of design efficiency and beamforming capabilities, respectively. We restrict our analyses to a linear array due to the computational cost of the FDFD solver. In the absence of mutual coupling effects as in our design, a planar array can be considered a combination of two linear arrays [11], and therefore the analyses presented completely characterize performance metrics.

A. Single Element Design Efficiency

We present the derived relation between the Fermi energy of the graphene stub and the relative phase delay in Fig. 3(a). It is seen that within the range of 0.14 - $0.55\,\mathrm{eV}$ (a smaller range compared to the other related works [17]–[19]), continuous and complete phase control is achieved.

Figure 3(b) compares the magnitude of reflection of the hybrid element with that of metallic and graphene patches, all resonant at the same frequency (1.5 THz). It is seen that the metallic patch provides the strongest reflection, but does not have any tunability. The graphene patch suffers a severely weakened reflected signal due to mismatch in the momentum of SPP and EM waves, as previously discussed. The hybrid element has slight power attenuation compared to the metallic patch due to power dissipation across the stub, but accommodates complete beamforming support.

B. Reflectarray Beamforming Capability

To determine the range of dynamic beamforming support provided by the reflectarray, a 4×1 reflectarray is analyzed.

Figure 4(a) presents the range of angles for which the designed reflectarray can comfortably steer a normally incident plane wave. It is seen that the hybrid reflectarray can provide up to 90° of continuous scanning across the broadside. Beyond this range, the limitations of the patch antenna start to manifest and result in truncated reflection strength [11], [12]. We exhibit the ability of the reflectarray to accommodate non-normal incident beams in Fig. 4(b). It is seen that for incident beams at as much as an angle of $\pm 45^\circ$ from the broadside, the reflectarray can direct the reflected beam broadside.

We highlight the ability of the reflectarray to engineer multi-purpose, multi-directional links in Fig. 5. It is seen that the reflectarray can direct an incident beam (at 30° in this case) towards multiple directions; specular (+30°), broadside (0°), retraced (-30°), or even to other arbitrary directions (such as $+45^\circ$ here). While the efficiency of the array is certainly diminished at the operational limits of beamsteering, this capability is essential to establish dynamic multipath links and help realize UM-MIMO at THz frequencies.

V. Conclusion

In this paper, we have proposed a novel metal/graphene hybrid reflectarray. We synergistically leverage the excellent reflection capabilities of micro-strip patches, and the excellent tunability of the graphene-based stub to engineer a smart reflectarray capable of creating multiple transmission paths through dynamic beamsteering. Our future work is aimed at fabricating and experimentally testing the proposed structure.

Acknowledgements

(a) Northeastern University acknowledges the U.S. Government's support in the publication of this paper. This material is based upon work funded by AFRL, under AFRL Grant No. FA8750-19-1-0502. (b) Any opinions, findings, and conclusions or recommendations expressed in this material are those of the author(s) and do not necessarily reflect the views of AFRL.

References

[1] R. Piesiewicz, T. Kleine-Ostmann, N. Krumbholz, D. Mittleman, M. Koch, J. Schoebei, and T. Kurner, "Short-range ultra-broadband terahertz communications: Concepts and perspectives," *IEEE Antennas and Propagation Magazine*, vol. 49, no. 6, pp. 24–39, 2007.

[2] T. S. Rappaport, Y. Xing, O. Kanhere, S. Ju, A. Madanayake, S. Mandal, A. Alkhateeb, and G. C. Trichopoulos, "Wireless communications and applications above 100 GHz: Opportunities and challenges for 6G and beyond," *IEEE Access*, vol. 7, pp. 78 729–78 757, 2019.

[3] I. F. Akyildiz, C. Han, and S. Nie, "Combating the distance problem in the millimeter wave and terahertz frequency bands," *IEEE Communications Magazine*, vol. 56, no. 6, pp. 102–108, 2018.

[4] I. F. Akyildiz and J. M. Jornet, "Realizing ultra-massive MIMO (1024×1024) communication in the (0.06–10) terahertz band," *Nano Communication Networks*, vol. 8, pp. 46–54, 2016, U.S. Patent No. 9,825,712, November 21, 2017 (Priority Date: Dec. 6, 2013).

[5] A. Tang, N. Chahat, Y. Zhao, G. Virbila, C. Lee, F. Hsiao, L. Du, Y.-C. Kuan, M.-C. F. Chang, G. Chattopadhyay *et al.*, "A 65nm cmos 140 ghz 27.3 dbm eirp transmit array with membrane antenna for highly scalable multi-chip phase arrays," in *2014 IEEE MTT-S International Microwave Symposium (IMS2014)*. IEEE, 2014, pp. 1–3.

[6] K.-M. Luk, S.-F. Zhou, Y. Li, F. Wu, K.-B. Ng, C.-H. Chan, and S. Pang, "A microfabricated low-profile wideband antenna array for terahertz communications," *Scientific reports*, vol. 7, no. 1, p. 1268, 2017.

[7] D. Headland, Y. Monnai, D. Abbott, C. Fumeaux, and W. Withayachumnankul, "Tutorial: Terahertz beamforming, from concepts to realizations," *Apl Photonics*, vol. 3, no. 5, p. 051101, 2018.

[8] A. K. Geim and K. S. Novoselov, "The rise of graphene," in *Nanoscience and Technology: A Collection of Reviews from Nature Journals*. World Scientific, 2010, pp. 11–19.

[9] H. Sarieddeen, M.-S. Alouini, and T. Y. Al-Naffouri, "Terahertz-band ultra-massive spatial modulation mimo," *arXiv preprint arXiv:1905.04732*, 2019.

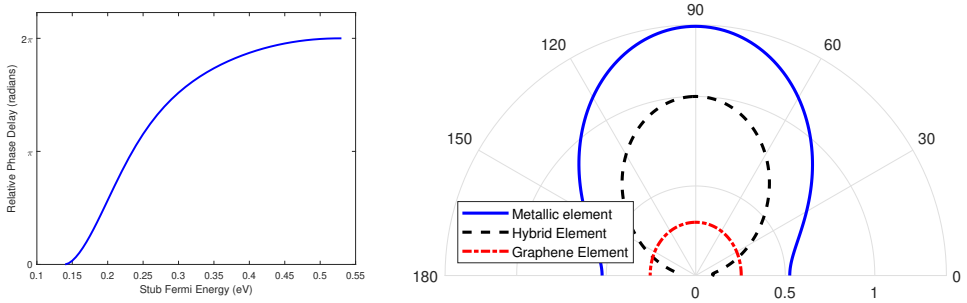

(a) Phase derivation (b) Radiation efficiency

Fig. 3: Single element efficiency: a) Available phase range; and b) Comparison of the radiation strength.

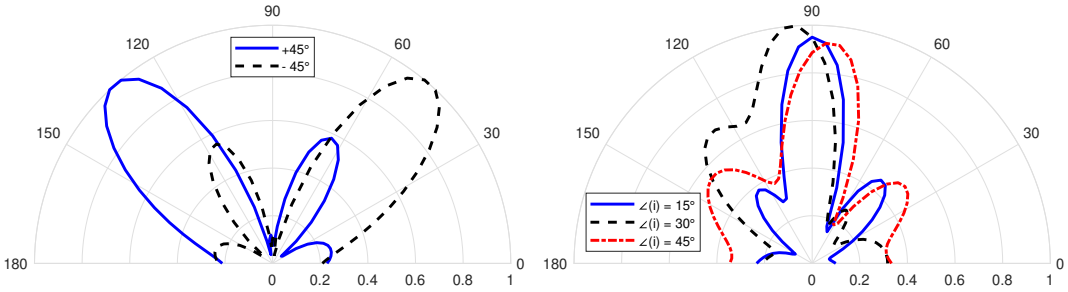

(a) Scanning range (b) Broadside directivity

Fig. 4: Dynamic beamforming support of the reflectarray: a) Scanning range; and b) Broadside directivity for different incident angles.

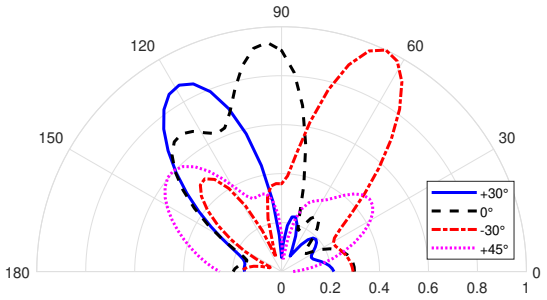

Fig. 5: Spatial coverage for a beam incident on the reflectarray at an angle of 30° from the broadside.

[10] S. Nie, J. M. Jornet, and I. F. Akyildiz, "Intelligent environments based on ultra-massive MIMO platforms for wireless communication in millimeter wave and terahertz bands," in *ICASSP 2019-2019 IEEE International Conference on Acoustics, Speech and Signal Processing (ICASSP)*. IEEE, 2019, pp. 7849–7853.

[11] C. A. Balanis, *Antenna theory: analysis and design*. John Wiley & Sons, 2016.

[12] N. Payam, Y. Fan, and A. Z. Elsherbeni, *Reflectaray Antennas: Theory, Designs, and Applications*. Wiley-IEEE Press, 2018.

[13] T. Niu, W. Withayachumnankul, B. S.-Y. Ung, H. Menekse, M. Bhaskaran, S. Sriram, and C. Fumeaux, "Experimental demonstration of reflectarray antennas at terahertz frequencies," *Optics Express*, vol. 21, no. 3, pp. 2875–2889, 2013.

[14] X. Tan, Z. Sun, D. Koutsonikolas, and J. M. Jornet, "Enabling indoor mobile millimeter-wave networks based on smart reflect-arrays," in *IEEE INFOCOM 2018 - IEEE Conference on Computer Communications*, April 2018, pp. 270–278.

[15] S. V. Hum and J. Perruisseau-Carrier, "Reconfigurable reflectarrays and array lenses for dynamic antenna beam control: A review," *IEEE Transactions on Antennas and Propagation*, vol. 62, no. 1, pp. 183–198, 2013.

[16] M. H. Dahri, M. H. Jamaluddin, M. Khalily, M. I. Abbasi, R. Selvaraju, and M. R. Kamarudin, "Polarization diversity and adaptive beamsteering for 5g reflectarrays: A review," *IEEE Access*, vol. 6, pp. 19 451–19 464, 2018.

[17] E. Carrasco, M. Tamagnone, and J. Perruisseau-Carrier, "Tunable graphene reflective cells for THz reflectarrays and generalized law of reflection," *Applied Physics Letters*, vol. 102, no. 10, p. 104103, 2013.

[18] Z. Chang, L.-S. Wu, M. Tang, Y.-P. Zhang, and J.-F. Mao, "Generation of thz wave with orbital angular momentum by graphene patch reflectarray," in *2015 IEEE MTT-S International Microwave Workshop Series on Advanced Materials and Processes for RF and THz Applications (IMWS-AMP)*. IEEE, 2015, pp. 1–3.

[19] X. B. Li, W. B. Lu, J. Wang, B. H. Huang, and H. Chen, "Dual-beam scanning using graphene-based reflectarray," in *2015 Asia-Pacific Microwave Conference (APMC)*, vol. 2. IEEE, 2015, pp. 1–3.

[20] P. K. Singh, G. Aizin, N. Thawdar, M. Medley, and J. M. Jornet, "Graphene-based plasmonic phase modulator for terahertz-band communication," in *Proc. of the 10th European Conference on Antennas and Propagation (EuCAP)*. IEEE, 2016, pp. 1–5.

[21] V. Ryzhii, "Terahertz plasma waves in gated graphene heterostructures," *Japanese Journal of Applied Physics*, vol. 45, 2008.

[22] G. W. Hanson, "Dyadic green's functions and guided surface waves for a surface conductivity model of graphene," *Journal of Applied Physics*, vol. 103, no. 6, p. 064302, 2008.

[23] A. S. Mayorov, R. V. Gorbachev, S. V. Morozov, L. Britnell, R. Jalil, L. A. Ponomarenko, P. Blake, K. S. Novoselov, K. Watanabe, T. Taniguchi *et al.*, "Micrometer-scale ballistic transport in encapsulated graphene at room temperature," *Nano letters*, vol. 11, no. 6, pp. 2396–2399, 2011.

[24] J. M. Jornet and I. F. Akyildiz, "Graphene-based nano-antennas for electromagnetic nanocommunications in the terahertz band," in *Proceedings of the Fourth European Conference on Antennas and Propagation*. IEEE, 2010, pp. 1–5.